Effects of thermal conductivity of airframe substrate on the dynamic ice accretion process pertinent to UAS inflight icing phenomena

Linkai Li, Yang Liu, Zichen Zhang, Hui Hu *

Department of Aerospace Engineering, Iowa State University, 537 Bissell Road, Ames, IA 50011-1096, USA

ARTICLE INFO

ABSTRACT

An experimental investigation was conducted to quantify the dynamic ice accretion and the unsteady heat transfer process over the ice accreting surfaces of composite-based airframes widely used for light-weight, Unmanned-Aerial-Systems (UAS), in comparison to those over the surfaces of metal-based airframes used by conventional manned aircraft, in order to elucidate the underlying icing physics specifically pertinent to UAS inflight icing phenomena. Two airfoil/wing models with the same airfoil shape, but made of different materials (i.e., thermoplastic material with the thermal conductivity being only $\sim$0.2 W/m·K to represent typical UAS airframe substrates vs. Aluminum with the thermal conductivity being $\sim$200 W/m·K widely used for conventional manned aircraft). The two test models were mounted side-by-side inside an Icing Research Tunnel available at Iowa State University (i.e., ISU-IRT) under the same wet glaze or dry rime icing condition. During the icing experiment, while a high-speed imaging system was used to record the dynamic ice accretion process over the surfaces of the test models, an infrared thermal imaging system was also used to map the corresponding surface temperature distributions over the ice accreting airfoil surfaces. It was found that, upon the impacting of the airborne, super-cooled water droplets in ISU-IRT, ice would start to accrete rapidly on the surfaces of the test models with a significant amount of the latent heat of fusion being released associated with the phase changing of the impacted super-cooled water mass over the airfoil surfaces. The thermal conductivity of the airframe substrate was found to affect the dynamic ice accretion and unsteady heat transfer processes over the ice accreting surfaces significantly. With the two test models being exposed under the same icing conditions, the released latent heat of fusion was found to be dissipated much slower over the surface of the thermoplastic model, due to the much lower thermal conductivity of the thermoplastic substrate. In comparison with those on the surface of the Aluminum model, the slower dissipation of the released latent heat of fusion on the surface of the thermoplastic model was found to cause higher surface temperatures and greater "heated" regions near the airfoil leading edge, more obvious surface water run-back over the airfoil surface, and formation of more complex rivulet-shaped ice structures at further downstream locations beyond the direct impinging zone of the super-cooled water droplets.

© 2018 Elsevier Ltd. All rights reserved.

1. Introduction

Unmanned Aerial System, i.e., UAS in short, is one of the most remarkable developments in aviation in recent years. These remotely—or sometimes autonomously—controlled vehicles have become invaluable tools for various civilian and military applications, including reconnaissance and combat, cargo transport, search and rescue, and wildfire monitoring. Free from having to accommodate the safety needs and endurance limits of onboard pilots, UAS is capable of flying extended missions and venturing into hazardous and remote locations. Additionally, the associated cost savings and casualty reduction in using UAS for various military reconnaissance and surveillance operations are also very attractive, in comparison to conventional manned aircraft. As a result, military operations in the Balkans, Afghanistan and Iraq have seen a widespread use of UASs such as Global Hawk, Predator and Phoenix [1].

Aircraft inflight icing is one common aviation danger that plagues both unmanned and manned airplanes flying in cold climates. In comparison with conventional, large-sized, manned aircraft, light-weight UAS is more susceptible to inflight icing problems due to the lower cruising altitude with relatively higher liquid water content (LWC) and relatively warmer air temperatures to

---

cause glaze ice formation, smaller excess power margin to offset the increased drag caused by ice accretion, lower flying velocity to result in longer exposing to icing conditions, and more damage to important sensors onboard [2]. The potential damage of inflight icing to UAS renders their operations unfeasible in cold weather. As described in Botura and Fahrner [3], 25% UAS flights encountered ice during a specific military operation that has negatively impacted the success of the mission. The common icing avoidance strategies for UAS are keeping the aircraft on the ground [4] or modifying path planning [5], which would greatly reduce the operation capability of UAS in cold climates. This is particularly troubling for military UAS applications, in which icing conditions can lead to mission aborts and the loss of crucial tactical capabilities.

While a number of anti-/de-icing solutions, such as freezing point depressants, pneumatic boots, warm air blowing, and electric heater, have been successfully applied on conventional, large-sized, manned aircraft [6,7], those traditional anti-/de-icing methods can be too complex, too heavy or draw too much power to be effective, therefore, might not be applicable to small, light-weight UAS, due to the limited payload and scant excess power. Advancing the technology for safer and more efficient UAS operations in atmospheric icing conditions requires the development of innovative, effective anti-/de-icing strategies tailored specifically for UAS icing mitigation and protection. Doing so requires a keen understanding of the underlying physics of complicated thermal flow processes pertinent to UAS icing phenomena. While several studies have been carried out recently to simulate ice formation and accretion on airfoil/wing models through icing tunnel testing [8,9] or using "artificial" iced profiles with various types and amounts of ice accretion to investigate the aerodynamic performance degradations of iced airfoils/wings [10–12], most of the previous studies were targeted for the anti-/de-icing of conventional, large-sized manned aircraft. In comparison to those of manned aircraft with much larger size and higher flight speed, thereby, much higher Reynolds numbers, many special issues related to inflight icing phenomena on UAS with much smaller size, lower flying speed, and lower Reynolds numbers have not been fully explored. For example, different from traditional, large-sized, manned aircraft with airframes typically being made of metals (e.g., aluminum and/or aluminum alloy), most of UAS airframes are made of polymer-based composites. While local heat transfer to remove the released latent heat of fusion from the ice accreting surface is one of the key controlling factors to determine ice types (i.e., rime vs. glaze) and ice accretion rate, the effects of the significant difference in thermal conductivity between the traditional metal-based airframes (i.e., ~200 W/m·K) and the composite-based surfaces (i.e., only ~0.2 W/m·K) on the ice accretion process are still unclear.

In the present study, an experimental investigation was conducted to quantify the dynamic ice accretion and unsteady heat transfer process over the surface of a typical composite-based UAS airfoil/wing model, in comparison to that over the surface of a conventional metal-based airfoil/wing model, to elucidate the underlying physics pertinent to UAS inflight icing phenomena. The experimental study was performed in the unique Icing Research Tunnel of Iowa State University (i.e., ISU-IRT). Two airfoil/wing models with the same airfoil shape and the same chord length, but being made of different materials (thermoplastics vs. Aluminum), were used for the comparative study to evaluate the effects of the thermal conductivity of the airframe substrates on the dynamic ice accretion and unsteady heat transfer processes over the airfoil surfaces of the two compared test models. While the airfoil/wing model being made of thermoplastic material (i.e., the thermal conductivity of the substrate being ~0.2 W/m·K) is used to represent the composites-based UAS airframes, the

Aluminum model (i.e., the thermal conductivity being ~200 W/m·K for the Aluminum airframe substrate) are used to be the representative of the airframes used for traditional, large-sized manned aircraft. During the experiments, in addition to revealing the time evolution of the dynamic ice accretion process over the surfaces of the airfoil/wing models with a high-speed imaging system, an infrared (IR) thermal imaging system was also utilized to measure the corresponding surface temperature distributions over the ice accreting airfoil surfaces. Based on the time sequences of the acquired snapshots of the ice accretion images and the spatially-and-temporally-resolved surface temperature measurements, the characteristics of the dynamic ice accretion and unsteady heat transfer processes on the surfaces of the two compared airfoil/wing models, i.e., with different thermal conductivities of the airframe substrates, were examined quantitatively under typical wet glaze and dry rime icing conditions.

2. Test models and experimental setup

The experimental study was performed in the unique Icing Research Tunnel located at Aerospace Engineering Department of Iowa State University (i.e., ISU-IRT). As shown schematically in Fig. 1, the ISU-IRT is a research-grade, multi-functional icing tunnel with a test section of 2.0 m in length × 0.4 m in width × 0.4 m in height with four side walls being optically transparent. It has a capacity of generating a maximum wind speed of 60 m/s and an airflow temperature down to −25 °C. An array of 8 pneumatic atomizer/spray nozzles are installed at the entrance of the contraction section of ISU-IRT to inject micro-sized water droplets (10–100 μm in size with MVD being ~20 μm) into the airflow. By manipulating the water flow rate through the spray nozzles, the liquid water content (LWC) in ISU-IRT can be adjusted (i.e., LWC ranging from 0.1 g/m³ to 10.0 g/m³). In summary, ISU-IRT can be used to simulate various atmospheric icing phenomena over a wide range of icing conditions (i.e., from dry *rime* to extremely wet *glaze* ice conditions). Further information about ISU-IRT can be found at Waldman & Hu [13] and Liu & Hu [14]

In the present study, two airfoil/wing models with the same NACA0012 airfoil shape and the same chord length of C = 150 mm, but being made of different substrate materials, were manufactured for the comparative study to evaluate the effects of the thermal conductivity of the airframe substrates on the dynamic ice accretion and unsteady heat transfer processes over the airfoil/wing surfaces. One of the airfoil/wing models, which is used to represent the composites-based UAS airframes, is made of thermoplastic material (i.e., ULTEM®1010) and manufactured by using a rapid prototyping machine (i.e., 3-D printing) that builds the 3-D model layer-by-layer with a resolution of about 50 μm. The surface of the thermoplastic model was wet-sanded by using a series of progressively finer sandpapers (up to 2000 grit) to achieve a very smooth, glossy finish with a characteristic roughness of about 20 μm. According to the MSDS of the thermoplastic material available online at https://www.sabic.com/en/products/specialties/ultem-resins/ultem-resin, the thermal conductivity of the thermoplastic material is 0.22 W/m·K. The second airfoil/wing model is made of Aluminum (i.e., 6061 Aluminum) by using a CNC (Computer Numeric Control) machine, which is used to represent traditional metal-based airframes of large-sized manned aircraft. According to the thermophysical properties data of metallic solids listed in the textbook of Incropera & DeWitt [15], the thermal conductivity of 6061 Aluminum is about 200 W/m·K, which is about 1000 times greater than that of the thermoplastic material. As shown schematically in Fig. 1, the two models were mounted side-by-side and oriented horizontally in the middle of the
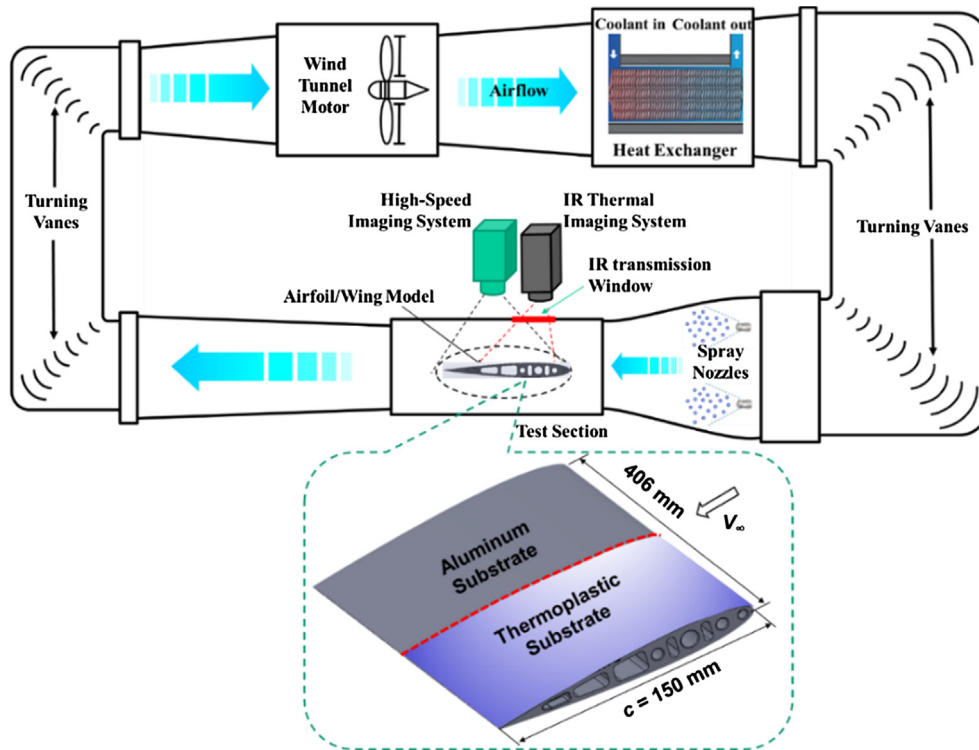
Fig. 1. A schematic of the experimental setup used in the present study.

ISU-IRT test section with the angle of attack (AOA) of the airfoil/wing models being zero (i.e., AOA = 0.0°).

It should be noted that, the surface wettability of an airfoil/wing model may also affect the dynamic ice accretion process, as reported in the recent studies of Antonini et al. [16] and Yang et al. [17]. By using the similar procedure as that described in Waldman et al. [18], the static contact angles of sessile water droplets on the surfaces of the test plates made of the thermoplastic material ULTEM®1010 and 6061 Aluminum were measured. The receding and advancing angles of water droplets (i.e., $\theta_{advancing}$ and $\theta_{receding}$) over the surfaces of the two compared materials were also measured quantitatively by using a needle-in-the-sessile-drop method as that described in Korhonen et al. [19]. As shown clearly in Fig. 2, the static contact angles of the water droplets sitting on the surfaces of the thermoplastic material and the 6061 Aluminum were found to be smaller than 90° ($\theta_{static} < 90°$), demonstrating hydrophilic nature of the surfaces. Table 1 summarizes the measured static contact angles θ_{static}, advancing contact angle θ_{adv}, and receding contact angle $\theta_{rec.}$ along with the corresponding hysteresis $\Delta\theta$ of the two compared materials. It can be seen clearly that, in addition to the fact that the thermoplastic material of ULTEM®1010 and the 6061 Aluminum are hydrophilic with almost

Table 1
The thermal conductivity and surface wettability of the two compared substrate materials.

Measured Parameters		Thermoplastic ULTEM®1010	6061 Aluminum
Thermal Conductivity, k (W/m·K)		0.22	200
Surface wettability	Static CA θ_{static} (°)	80 ± 3.4	84 ± 4.2
	Advancing CA θ_{adv} (°)	97 ± 0.6	92 ± 3.9
	Receding CA θ_{rec} (°)	20 ± 6.0	24 ± 2.0
	Hysteresis $\Delta\theta = \theta_{adv} - \theta_{rec}$ (°)	77 ± 6.4	68 ± 5.3

the same static contact angles θ_{static}, the receding and advancing angles of water droplets (i.e., θ_{adv} and θ_{rec}) on the surfaces of the two compared substrate materials were also found to be very close to each other. In summary, the two compared substrates of the airfoil/wing models used in the present study were found to have very similar surface wettability. Therefore, the effects of the differences in the surface wettability of the two test models on the dynamic ice accretion processes are expected to be relatively small, which is negligible for the test cases of the present study.
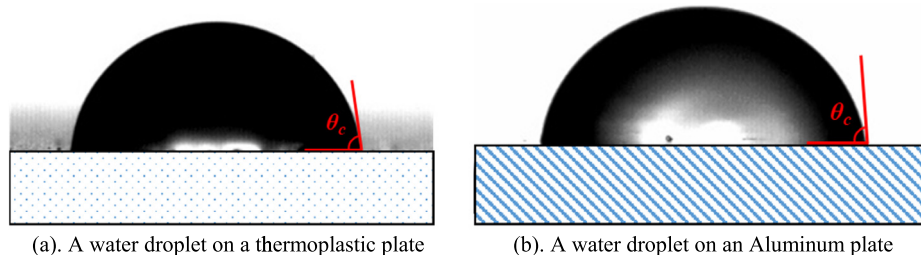

(a). A water droplet on a thermoplastic plate

(b). A water droplet on an Aluminum plate

Fig. 2. The contact angles of water droplets sitting over the surfaces of the two compared substrate materials.

During the icing experiment, a high-resolution, high-speed imaging system (i.e., PCO Tech, Dimax^{TM} camera with 2000 pixels by 2000 pixels and frame rate of up to 10,000 frames per second) was used to record the dynamic ice accretion process over the surfaces of the two test models. The high-speed camera was installed at about 500 mm above the airfoil/wing model with a 60 mm lens (Nikon, 60 mm Nikkor 2.8D). The camera was positioned approximately normal to the chords of the airfoil/wing models with a measurement window of 210×210 mm^2 (i.e., the resolution of the acquired images being 9.5 pixels/mm). In addition to the high-speed imagining system (i.e., video camera), an Infrared (IR) thermal imaging system (FLIR-A615 with 640 pixels $\times$ 480 pixels in spatial resolution) was also utilized in the present study to map the surface temperature distributions over the ice accreting airfoil surfaces via an IR transmission window mounted on the upper wall of ISU-IRT test section. The IR thermal imaging system adopts a new interface standard of GigE Vision that allows for fast image transfer to achieve 16-bit thermal imaging outputs at frame rates up to 200 Hz. The IR thermal imaging camera was mounted at 450 mm above the airfoil/wing models. A calibration procedure similar as that described in Liu et al. [14] was performed to calibrate/validate the IR thermal imaging system for the surface temperature measurements of the airfoil/wing models at several prescribed low temperatures (i.e., ranged from −20 °C to 0 °C). After carefully calibrated and validated, the IR thermal imaging system was then used to map the surface temperature distributions over the ice accreting airfoil surfaces under different icing conditions. The temperatures of the incoming airflow and the surface temperatures of the airfoil/wing models were also monitored by using thermocouple probes. During the icing experiments, a hair dryer was used to blow dry warm air flowing gently along the outer wall of the observation window to avoid the fog formation for the high-speed video acquisition. A layer of dry gas film (i.e., at room temperature) supplied by using a pressurized gas cylinder was generated to cover the outer wall of the IR transmission window to prevent the fog formation for the IR thermal image acquisition. Both the high-speed video camera and the IR thermal imaging system were synchronized with the electric switch of the water spray system of ISU-IRT so that the dynamic ice accreting process (i.e., impacting dynamics of the super-cooled water droplets, transient water film/rivulets runback, and dynamic ice accretion process) over the surfaces of the airfoil/wing models can be revealed clearly and quantitatively from the acquired snapshots of the high-speed video camera and the surface temperature measurement results of the IR thermal imaging system.

3. Theoretical analysis of the effects of the thermal conductivity of airframe substrate on the dynamic ice accretion process over an airfoil surface

In the present study, a theoretical model is developed to analyze the characteristics of the unsteady heat transfer during the dynamic ice accretion process over an airfoil/wing surface. As shown schematically in Fig. 3, energy conservation law is applied to an arbitrarily-selected control volume over an ice accreting airfoil surface. During the dynamic ice accretion process, the rate at which the thermal and/or mechanical energies enter or leave from the control volume would be balanced by the rate of the net energy increase stored/released within the control volume:

$$\dot{E}_{st} = \frac{dE_{st}}{dt} = \dot{E}_{in} - \dot{E}_{out} \qquad (1)$$

The energy change stored within the control volume is essentially due to the changes in the internal, kinetic, and/or potential energies of its contents:

$$\Delta E_{st} = \Delta U + \Delta KE + \Delta PE \qquad (2)$$

where ΔU, ΔKE, and ΔPE are representing the changes in the internal energy, kinetic energy, and potential energy.

As described in Liu & Hu [14], during the dynamic ice accretion process, the changes of kinetic and potential energy inside the control volume are usually several orders of magnitude smaller than the change of internal energy, thereby, can be neglected. When super-cooled water droplets impinge onto the airfoil/wing surfaces, there will be a phase transition of the super-cooled water droplets from liquid into solid state to give off energy (i.e., known as the latent heat of fusion) due to the changes in the intermolecular forces, and less from a sensible component that accounts for the motion of the atoms/molecules. Thus, the net energy stored inside the control volume is reduced, which can be expressed as:

$$\frac{dE_{st}}{dt} = -\left(\dot{Q}_{latent} + \dot{Q}_{ss} \right) \qquad (3)$$

where Q_{latent} is the latent heat of fusion, Q_{ss} is the sensible heat.

While the energy inputs are mainly contributed by the kinetic energy of the surface water flowing into the control volume (i.e., run-in water), the energy outputs are dominated by the heat convection, the heat conduction and the kinetic energy of the runback water leaving the control volume. Thus, the energy conservation equation of the control volume can be expressed as:

$$\dot{Q}_{run-in} - \left(\dot{Q}_{conv} + \dot{Q}_{cond} + \dot{Q}_{runback} \right) = -\dot{Q}_{latent} \qquad (4)$$

which can be further formulated as:

$$\dot{Q}_{run-in} + \dot{Q}_{latent} = \dot{Q}_{conv} + \dot{Q}_{cond} + \dot{Q}_{runback} \qquad (5)$$

The kinetic energy of the surface water flowing into the control volume can be expressed as:

$$\dot{Q}_{run-in} = \frac{1}{2} \cdot \dot{m}_{run-in} \cdot V_{run-in}^2 \qquad (6)$$

where $\dot{m}_{run-in}$ is the mass flux of the surface water flowing into the control volume (i.e., run-in water), V_{run-in} is the velocity of the surface water.

The heat flux due to the latent heat of fusion released within the control volume is dependent on the freezing rate of the super-cooled surface water, which can be written as:

$$\dot{Q}_{latent} = \dot{m}_{ice} \cdot L_s \qquad (7)$$

where $\dot{m}_{ice}$ is the freezing rate of surface water (i.e., ice accretion rate) in the control volume, and L_s is the latent heat released per unit water mass.

Convective heat transfer would occur as the airflow moving over the airfoil/wing surface. As described in the textbook of Incropera & DeWitt [15], the heat convection term in the energy equation can be expressed as:

$$\dot{Q}_{conv} = h_{cv} \cdot (T_{surface} - T_{\infty}) \cdot A_{convection} \qquad (8)$$

where h_{cv} is the convective heat transfer coefficient, $T_{surface}$ is the surface temperature of the accreted ice layer, T_{∞} is the temperature of the incoming airflow, and $A_{convection}$ is the interface area of the air/water or air/ice within the control volume.

Conductive heat transfer would also occur at the interface between the ice/water and the airframe substrate of the airfoil/wing model. The heat flux due to the thermal conduction is given as:

$$\dot{Q}_{cond} = \frac{(T_{surface} - T_{airframe}) \cdot A_{conduction}}{R_{conduction}} \qquad (9)$$

where $T_{airframe}$ is the surface temperature of the airfoil substrate, $A_{conduction}$ is the interface area of the air/water and airframe substrate
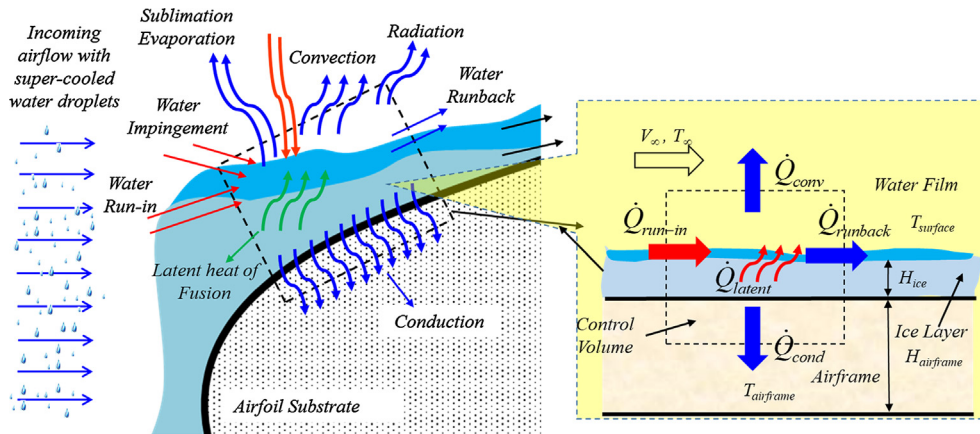
Fig. 3. A schematic of the unsteady heat transfer process over the airfoil/wind surface.

within the control volume. $R_{conduction}$ is the equivalent thermal resistance for the heat conduction, which can be derived based on the equivalent thermal circuit theory as described in Incropera & DeWitt [15]:

$$R_{conduction} = \frac{H_{ice}}{k_{ice}} + \frac{H_{airframe}}{k_{airframe}} \qquad (10)$$

where H_{ice} is the thickness of the accreted ice layer, and $H_{airframe}$ is the airframe thickness, k_{ice} and $k_{airframe}$ are the thermal conductivities of the ice layer and the airframe substrate, respectively.

During the ice accretion process, especially under glaze icing condition, if impacted water mass could not be frozen immediately upon impacting of the super-cooled water droplets onto the airfoil/wing surface, there would be surface water runback on the surface of the airfoil/wing model. The kinetic energy of the runback surface water leaving the control volume can be expressed as:

$$\dot{Q}_{runback} = \frac{1}{2} \cdot \dot{m}_{runback} \cdot V_{runback}^2 \qquad (11)$$

where $\dot{m}_{runback}$ is the mass flux of runback water and $V_{runback}$ is the runback velocity of the surface water.

By substituting Eqs. (6)(11) into Eq. (5), the energy conservation equation can be expressed as following:

$$\frac{1}{2} \cdot \dot{m}_{run-in} \cdot V_{run-in}^2 + \dot{m}_{ice} \cdot L_s = h_{cv} \cdot (T_{surface} - T_\infty) \cdot A_{convection}$$
$$+ \frac{(T_{surface} - T_{airframe}) \cdot A_{conduction}}{R_{conduction}}$$
$$+ \frac{1}{2} \cdot \dot{m}_{runback} \cdot V_{runback}^2 \qquad (12)$$

During the ice accretion process, the conservation equation of water mass within the control volume can be expressed as following:

$$\dot{m}_{run-in} = \dot{m}_{ice} + \dot{m}_{runback} \qquad (13)$$

As the control volume is relatively small, the velocity of the surface water running into the control volume can be assumed to be almost the same as that running out of the control volume, i.e., $V_{run-in} \approx V_{runback}$.

Therefore, the water freezing rate or ice accretion rate within the control volume can be derived as following:

$$\dot{m}_{ice} = \frac{h_{cv} \cdot (T_s - T_\infty) \cdot A_{convection} + [(T_s - T_{airframe}) \cdot A_{conduction}/R_{conduction}]}{L_s + 0.5 \cdot V_{runback}^2}$$
$$(14)$$

As described above, the ice accretion rate over an airfoil/wing surface would be closely related to the heat convection and heat conduction during the ice accretion process. In the present study, since the incoming airflow conditions and the airfoil shape were set to be the same for the two compared airfoil/wing models, the convective heat transfer process over the ice accreting airfoil surfaces of the two test models are expected to be very similar during the ice accretion experiment. Therefore, the differences in the dynamic ice accretion processes over the surfaces of the test models would be mainly due to the differences in the heat conduction via the airframe substrates of the models.

Based on the simplified heat transfer model given in Eq. (14), the ice accretion rate over the airfoil/wing surfaces would highly depend on the thermal resistance of the heat conduction $R_{conduction}$ (i.e., $\dot{m}_{ice} \propto 1/R_{conduction}$). At the early stage of the ice accretion process (i.e., within the first ~ 60 s of the ice accretion experiment for the present study), the thickness of the ice layer accreted over the airfoil surface would be much smaller in comparison with the airframe thickness (i.e., $H_{ice} \ll H_{airframe}$), thus, the thermal resistance of the heat conduction given in Eq. (10) can be simplified as $R_{conduction} \approx H_{airframe}/k_{airframe}$. Then, the Eq. (14) can be re-written as:

$$\dot{m}_{ice} = \frac{h_{cv} \cdot (T_s - T_\infty) \cdot A_{convection}}{L_s + 0.5 \cdot V_{runback}^2}$$
$$+ \frac{(T_s - T_{airframe}) \cdot A_{conduction}/H_{airframe}}{L_s + 0.5 \cdot V_{runback}^2} k_{airframe} \qquad (15)$$

Therefore, the ice accretion rate over the airfoil/wing surfaces at the early stage of the icing experiment would highly depend on the thermal conductivity of the airframe substrates of the test models. More specifically, the ice accretion rate $\dot{m}_{ice}$ within the control volume would increase monotonically with the thermal conductivity of the airframe substrate $k_{airframe}$. It implies that, as the thermal conductivity of the substrate increases, more surface water would be frozen into solid ice within the control volume, thereby, less surface water flowing out of the control volume (i.e., less water runback). Therefore, with the two compared airfoil/wing models being exposed under the same icing conditions (i.e., with the same amount of super-cooled water droplets impinging onto the surfaces of the airfoil/wing models), more obvious surface water runback and formation of glaze ice structures are expected on the surface of the test model being made of thermoplastic material (i.e., with much smaller thermal conductivity of $k_{TP} = 0.22$ W/m·K), in comparison to that of the aluminum model with much higher thermal conductivity (i.e., $k_{AL} = 200$ W/m·K) for the airframe

substrate, which were revealed clearly from the snapshot images of the dynamic ice accretion process recorded by using the high-speed video camera and the IR thermal imaging system to be presented in the next section.

4. Experimental results and discussions

It is well known that ice accretion process over UAS airframe surfaces can be either wet (i.e., glaze ice) or dry (i.e., rime ice), depending on the ambient icing conditions [20]. When an UAS encounters clouds with low liquid water content (LWC) levels at relatively low ambient temperatures (i.e., typically below −8 °C), rime ice is usually formed as the super-cooled water droplets in the clouds would freeze immediately upon impacting onto the airframe surfaces. Glaze ice accretion is usually associated with warmer ambient temperatures (i.e., typically above −8°C) and at higher LWC levels of the clouds. In the present study, while the freestream velocity of the incoming airflow in ISU-IRT was kept at V_∞ = 40 m/s during the icing experiments, the LWC level in the incoming airflow was changed from LWC = 2.0 g/m³ to LWC = 1.0 g/m³, and the temperature of the incoming airflow was varied from T_∞ = −5 °C to T_∞ = −15 °C. With different settings of the test paradigms for the icing experiments, both rime and glaze ice accretion scenarios encountered within typical UAS flight envelopes were investigated in the present study.

In performing icing experiments, ISU-IRT was operated at a prescribed frozen-cold temperature level (e.g., T_∞ = −5° C or T_∞ = −15° C for the present study) for at least 20 min to ensure ISU-IRT reaching a thermal steady state. Since the temperature inside the ISU-IRT was well below the frozen temperature of water, the water droplets would be in a super-cooled state after exhausted from the spray nozzles of ISU-IRT. Upon impacting of the super-cooled water droplets onto the surfaces of the test models, dynamic ice accretion process would start to take place on the surfaces of the airfoil/wing models installed in the test section of ISU-IRT. The uniformity of the super-cooled water cloud in ISU-IRT was also validated carefully by checking the ice structures accreted over a mesh grid installed in the test section of ISU-IRT before conducting the ice accretion experiments.

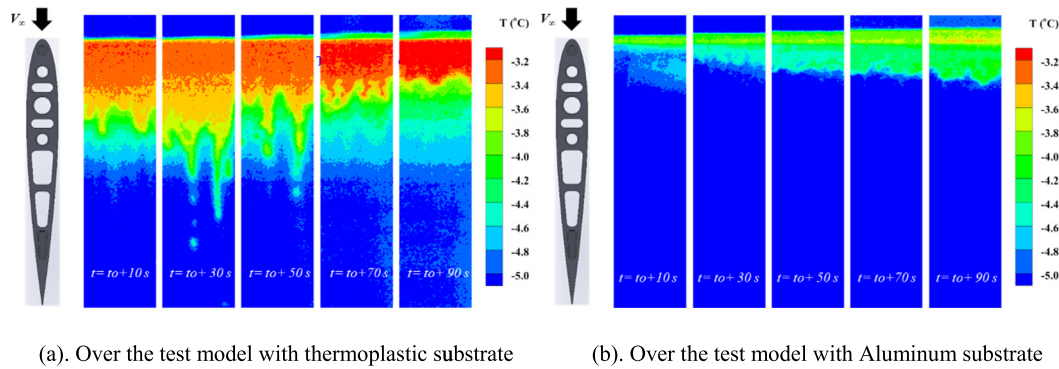### 4.1. Measurement results under a typical glaze icing condition

In the present study, ISU-IRT was used at first to generate a rather wet icing condition with the test paradigms being V_∞ = 40 m/s, T_∞ = −5 °C and LWC = 2.0 g/m³. Based on the recent icing experimental study as described in Waldman and Hu [13], a typical glaze ice accretion process would be expected over an airfoil surface under such a wet icing condition. Fig. 4 gives some typical snapshots of the images acquired by using the high-speed video camera to reveal the dynamic ice accretion processes over the surfaces of the two test models under the glaze icing condition. As described clearly in Liu and Hu [14], a significant amount of latent heat of fusion would be released associated with the phase changing of the impacted super-cooled water droplets, which causes the temperature increases over the ice accreting airfoil surfaces. Fig. 5 shows the corresponding surface temperature distributions measured by using the IR thermal imaging system, which can be used to characterize the unsteady heat transfer process over the ice accreting airfoil surfaces. It can be seen clearly that, upon the impacting of super-cooled water droplets onto the airfoil surfaces, ice structures were found to accrete immediately on the surfaces of the two test models. Since the latent heat of fusion was released associated with the phase changing (i.e., solidification) process of the impacted super-cooled water mass, the temperatures over the airfoil surfaces were found to rise rapidly due to the "heating effects" induced by the local "accumulation" of the released latent heat of fusion over the ice accreting surfaces of the test models.

As described in Liu & Hu [14], the type of ice accretion (i.e., rime vs. glaze) and growth rate of the ice structures accreted over an airframe surface would be mainly determined by the capacity to remove/dissipate the released latent heat of fusion over the ice accreting surface. Under the glaze icing condition with a relatively high LWC level in the incoming airflow (i.e., LWC = 2.0 g/m³), a large number of super-cooled water droplets would impact onto the surfaces of the test models after switching on the spray system of ISU-IRT for the icing experiment. A tremendous amount of latent heat of fusion would be released associated with the phase changing of the impacted super-cooled water mass over the surfaces of the test models. As described above, the released latent heat of fusion would be dissipated/removed by both heat convection (i.e., via the boundary layer airflows over the airfoil surfaces) and heat conduction (i.e., via the airframe substrates of the test models). Due to the relatively warm ambient temperature (i.e., T_∞ = −5°C) for the test case, the convective heat transfer (i.e., via the boundary layer airflow) over the airfoil surface would not be able to remove/dissipate all the released latent heat of fusion instantly, which causes the local "accumulation" of the released latent heat of fusion, thereby, surface temperature increases over the ice accreting airfoil surfaces. Beside the convective heat transfer via the boundary layer airflows, the conductive heat transfer via the airframe substrates of the test models could also play a very important role in dissipating/removing the released latent heat of fusion. Corresponding to the significant differences in the thermal conductivities between the thermoplastic material (i.e., k_{TP} = 0.22 W/m·K) and Aluminum (i.e., k_{AL} = 200 W/m·K), the capability of the conductive heat transfer via the airframe substrate in dissipating the released latent heat of fusion is expected to vary greatly for the two compared test models. In addition to the convective heat transfer via the boundary layer airflow over the airfoil surfaces, the released latent heat of fusion would also be dissipated rapidly

(a). Over the test model with thermoplastic substrate   (b). Over the test model with Aluminum substrate
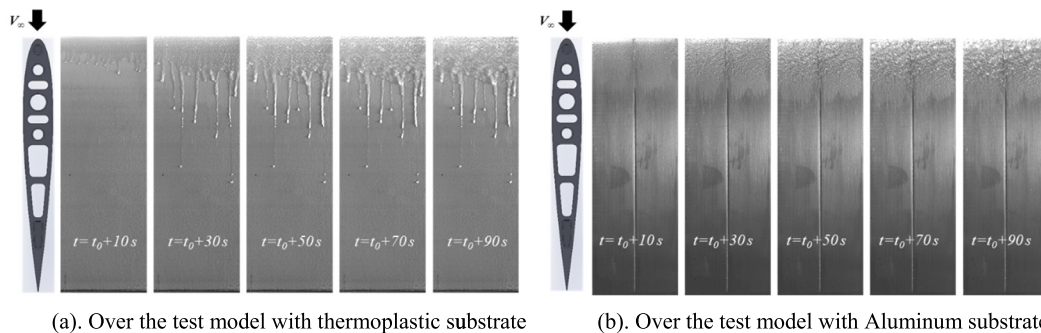
Fig. 4. Typical snapshots to reveal the dynamic ice accretion processes over the surfaces of the test airfoil/wing models under a typical glaze icing condition of V_∞ = 40 m/s, T_∞ = −5 °C, LWC = 2.0 g/m³.

(a). Over the test model with thermoplastic substrate   (b). Over the test model with Aluminum substrate

Fig. 5. Time evolution of the measured surface temperature distributions over the test airfoil/wing models under a typical glaze icing condition of V_∞ = 40 m/s, T_∞ = −5 °C, LWC = 2.0 g/m³.

by the conductive heat transfer via the airframe substrate for the Aluminum model. However, due to the nearly thermal isolation nature of the thermoplastic material, the released latent heat of fusion would hardly be dissipated via the thermoplastic substrate by the conductive heat transfer. As a result, even though the two test models were exposed under the same glaze icing condition of V_∞ = 40 m/s, T_∞ = −5 °C and LWC = 2.0 g/m³, the dynamic ice accretion process over the surfaces of the two compared test models were found to change significantly, as shown clearly in Figs. 4 and 5.
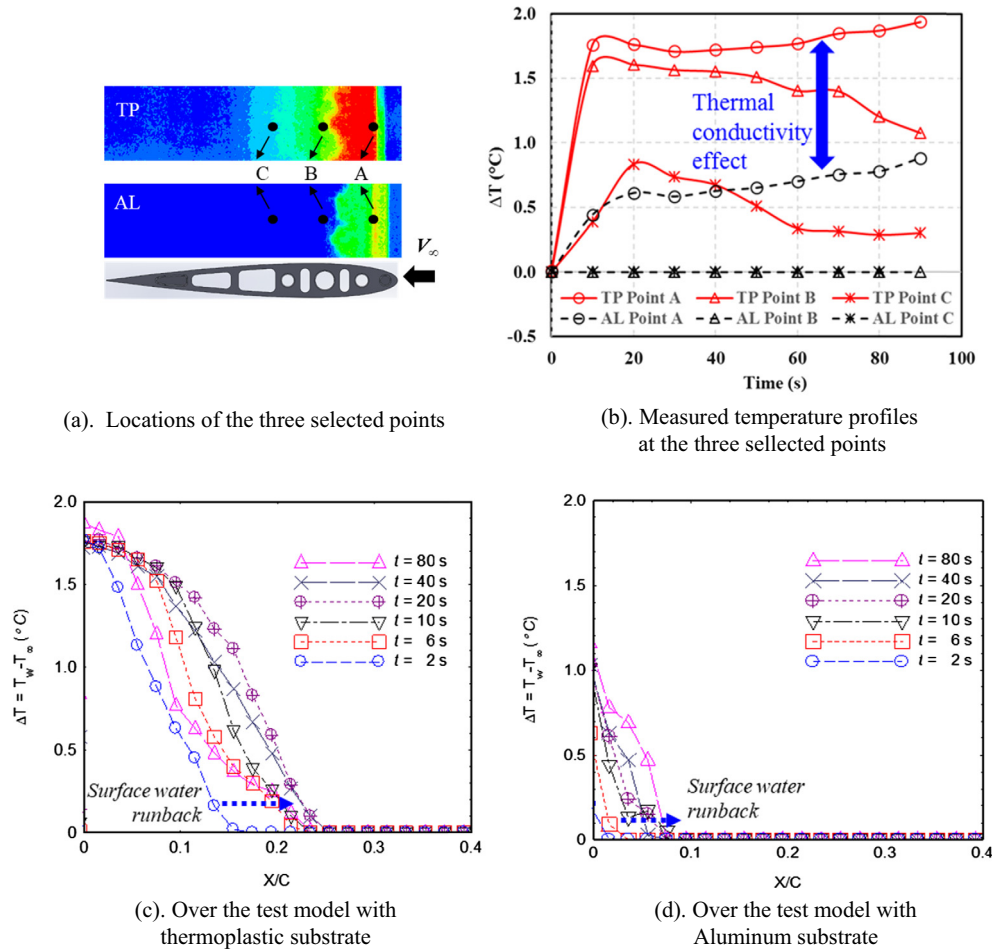
Since the released latent heat of fusion could not be dissipated instantly over the surface of the thermoplastic test model, only a portion of the impacted water mass would be frozen into ice immediately, while the rest of the impacted water mass was found to remain in the liquid phase over the airfoil surface. The unfrozen surface water was found to run back rapidly and reach further downstream locations, as driven by the boundary layer airflows over the airfoil surface. As a result, a typical glaze ice accretion process was found to take place over the surface of the thermoplastic model, i.e., obvious surface water runback and formation of rivulet-shaped ice structures were observed on the surface of the thermoplastic model, as shown clearly in Figs. 4(a) and 5(a).

With the Aluminum airfoil/wing model being exposed under the same glaze icing condition as that of the thermoplastic model, similar amount of the latent heat of fusion is expected to be released over the surface of the Aluminum test model as well. However, since the thermal conductivity of the Aluminum substrate is about 1000 times greater than that of the thermoplastic substrate, the dissipation of the released latent heat of fusion by conductive heat transfer would be much faster through the Alumina substrate, in comparison with that via the thermoplastic substrate. As predicted theoretically by the Eq. (11), more impacted water mass would be frozen into ice rapidly (i.e., with a much greater ice accretion rate) over the surface of the Aluminum model. It also indicates that much less impacted super-cooled water mass could remain in liquid phase due to the much faster dissipation of the released latent heat of fusion on the surface of the Aluminum test model. Therefore, much less obvious surface water runback and fewer rivulet-shaped ice structures were observed over the surface of the Aluminum model, in comparison with those over the surface of the thermoplastic model. The faster dissipation of the released latent heat of fusion over the Aluminum test model also resulted in much smaller surface temperature increases as well as the smaller size of the "heated" regions over the surface of the Aluminum model, which were revealed clearly and quantitatively from the acquired IR thermal images shown in Fig. 5.

Based on the time sequences of the acquired IR thermal images as those shown in Fig. 5, the time evolutions of the surface

temperature during the dynamic ice accretion process at representative locations over the surfaces of the two compared airfoil/wing model were extracted, and the results are shown in Fig. 6. As shown schematically in Fig. 6(a), the three representative points are selected in the middle planes of the test models, including Point "A" at the airfoil leading edge (i.e., at the location of X/C = 0); Point "B" at the 10% chord length downstream (i.e., at the location of X/C = 10%); and Point "C" at the 20% chord length downstream (i.e., at the location of X/C = 20%), respectively. The measured surface temperature profiles near the airfoil leading edges of the two test models (i.e., in the region of X/C < 40%) at different time instants during the icing experiment were also extracted, which are plotted in Fig. 6(c) and (d). By comparing the measured surface temperature increases (i.e., $\Delta T = T_W - T_\infty$; where T_W is the measured temperature on the ice accreting surfaces of the airfoil/wing models, T_∞ is the temperature of the incoming freestream airflow) over the surfaces of the two compared test models, the effects of the thermal conductivity of the airframe substrates on the dynamic ice accretion and unsteady heat transfer processes over the ice accreting surfaces can be revealed more clearly and quantitatively.

As described above, since ISU-IRT was operated at a pre-scribed frozen-cold temperature level (e.g., T_∞ = −5° C for the present test case) for at least 20 min to ensure the test models installed in ISU-IRT reaching a thermal steady state before switching on the water spray system, the surface temperatures of the test models were found to be the same as those of the incoming airflow (i.e., $\Delta T = T_W - T_\infty = 0$) before starting the ice accretion experiments. After the spray system of the ISU-IRT was turn on at the time instant of $t = 0$ s, the super-cooled water droplets carried by the incoming airflow would impact onto the surfaces of the test models within a narrow region near the airfoil leading edges (i.e., within the direct impinging zone of the super-cooled water droplets), as described in Papadakis et al. [21]. Latent heat of fusion was found to release instantly associated with the phase changing process of the impacted super-cooled water mass, causing the surface temperature increases near the leading edges of the ice accreting airfoil surfaces, as shown quantitatively in Fig. 6. Since the direct impingement region of the super-cooled water droplets over an airfoil surface would mainly concentrate within a narrow zone near the airfoil leading edge (i.e., mainly within the first ±5.0% of the airfoil chord, as described in Papadakis et al. [21]), only the surface temperature at the selected point "A", i.e., at the airfoil leading edge, was found to increase rapidly at the initial stage of the icing experiment (i.e., t < 1.0 s), while the surface temperature at the downstream locations (i.e., beyond the 10% of the airfoil chord at the selected points "B" and "C") were found to be unchanged

(a). Locations of the three selected points

(b). Measured temperature profiles at the three sellected points

(c). Over the test model with thermoplastic substrate

(d). Over the test model with Aluminum substrate

Fig. 6. Measured surface temperature profiles extracted from the IR thermal images for the test case under the glaze icing condition of V_∞ = 40 m/s, T_∞ = −5 °C and LWC = 2.0 g/m^3.

(i.e., $\Delta T = T_W - T_\infty = 0$) for both the compared test models at the initial stage of the icing experiment.

With continuous impingement of the super-cooled water droplets onto the test models, more and more impacted water mass would be collected over the airfoil surfaces to cause more and more released latent heat of fusion accumulated within the narrow region near the airfoil leading edge (i.e., within the direct impinging zone of the water droplets). As shown clearly in Fig. 6(b), the surface temperatures at the selected point "A" (i.e., at the airfoil leading edge) were found to increase monotonically at the beginning of the icing experiment for both the test models, until reaching an approximate thermal steady state at about t = 10–20 s. Since the conductive heat transfer via the airframe substrate of the Aluminum model would dissipate the released latent heat of fusion much faster than that via the thermoplastic substrate as described above, the temperature increase at the same selected point "A" was found to be much smaller on the Aluminum model, in comparison to that on the thermoplastic model. More specifically, the surface temperature increase at the selected point "A" was found to be less than $1.0\,°C$ (i.e., $\Delta T_A < 1.0\,°C$) on the Aluminum model at ~80 s after starting the icing experiment, whereas the corresponding value was found to become about $2.0\,°C$ (i.e., $\Delta T_A \approx 2.0\,°C$) on the thermoplastic model, as shown clearly in Fig. 6(b).

As described above, under the typical glaze icing condition, while tremendous latent heat of fusion was released corresponding to the relatively high LWC level in the incoming airflow (i.e., LWC = 2.0 g/m^3), the heat transfer process (i.e., by both the heat convection via the airflow and heat conduction via the airframe

substrates) could not dissipate/remove all the released latent heat of fusion instantly due to the relatively high ambient temperature (i.e., T_∞ = −5 °C for the test case). The released latent heat of fusion would be accumulated locally and caused a portion of the impacted super-cooled water mass to stay in the liquid phase. Due to the much smaller thermal conductivity of the thermoplastic material (i.e., k_{TP} = 0.22 W/m·K), the dissipation of the released latent heat of fusion on the surface of the thermoplastic model would be much slower than that on the surface of the Aluminum model. The slower dissipation of the released latent heat of fusion would enable a longer duration of the impacted super-cooled water mass staying in the liquid phase. As driven by the boundary layer airflow over the airfoil surface, the unfrozen surface water would run back quickly to reach much further downstream locations (i.e., far beyond the direct impinging zone of the super-cooled water droplets) before being frozen into solid ice eventually. As shown clearly in Fig. 6(b), due to the obvious runback of the unfrozen surface water, the surface temperatures at the selected points of "B" and "C" on the surface of the thermoplastic model were also found to increase gradually, and the surface temperature increases were found to become $\Delta T_B \approx 1.6\,°C$ and $\Delta T_C \approx 0.8\,°C$ at the time of $t \approx 20$ s, respectively. It should also be noted that, as shown clearly in Fig. 6(b), the surface temperatures at the points of "B" and "C" on the surface of the thermoplastic model were found to decrease gradually at the later stage of the icing experiment (i.e., at the time $t > 20$ s). The decreasing trend of the surface temperature at the further downstream locations (i.e., at the points of "B" and "C") observed at the later stage of

the icing experiment is believed to be closely related to the enhanced convective heat transfer caused by the formation of complex ice roughness over the iced airfoil surface, thereby, causing a faster dissipation of the released latent heat of fusion, as reported by Hawkins et al. [22].

For the scenario over the surface of the Aluminum test model, in addition to the convective heat transfer via the airflow over the airfoil surface, the conductive heat transfer via the Aluminum substrate could also promote a very fast dissipation of the released latent heat of fusion due to the much higher thermal conductivity of the Aluminum. Corresponding to the much faster dissipation of the released latent heat of fusion, the impacted super-cooled water mass would be frozen into ice much faster over the surface of the Aluminum model. The faster freezing process for the impacted water mass over the surface of the Aluminum model caused much fewer surface water to run back, thereby, much less ice formation at further downstream locations beyond the direct impinging zone of the super-cooled water droplets. As a result, the surface temperatures at the selected points of "B" and "C" on the surface of the Aluminum model were found to stay almost the same as the incoming freestream airflow (i.e., $\Delta T_B = \Delta T_C \approx 0.0 \,°C$) during the entire duration of the icing experiment. In comparison with those over the surface of the Aluminum model, the more obvious water runback and much greater surface temperature increases over the surface of the thermoplastic model were highlighted more clearly and quantitatively from the surface temperature distribution profiles measured at different time instants of the icing experiments, as those given in Fig. 6(c) and (d).

4.2. Measurement results under a typical rime icing condition

In the present study, the icing experiments were also conducted under a much colder and dryer icing condition (i.e., rime icing

condition) with the test parameters being $V_\infty = 40$ m/s, $T_\infty = -15\,°C$ and $LWC = 1.0$ g/m³. While Fig. 7 presents the typical snapshots acquired by using the high-speed imaging system to reveal the time evolution of the dynamic ice accretion process over the surfaces of the two test models, Fig. 8 illustrates the corresponding surface temperature distributions measured by the IR thermal imaging system. It can be seen clearly that, corresponding to the much colder ambient temperature (i.e., $T_\infty = -15\,°C$) and lower LWC level in the incoming airflow (i.e., $LWC = 1.0$ g/m³) under the rime icing condition, the super-cooled water droplets were found to be frozen into solid ice almost immediately upon impacting onto the surfaces of the test models. Instead of forming transparent, smooth-looking glazy ice structures as those shown in Fig. 4, much rougher and opaque ice layers were found to accumulate around the airfoil leading edges, i.e., ice accretion was found to be only within the direct impinging zone of the super-cooled water droplets without any noticeable surface water runback over the airfoil surfaces. Such experimental observations are of the typical characteristics of a rime icing process, as that described in Liu & Hu [14].

In comparison with those under the wet glaze ice accretion condition with a higher LWC level (i.e., $LWC = 2.0$ g/m³) and a warmer ambient temperature (i.e., $T_\infty = -5\,°C$) as described above, the incoming airflow would contain much fewer super-cooled droplets under the rime icing condition, corresponding to the lower LWC level (i.e., $LWC = 1.0$ g/m³). Therefore, a smaller amount of the super-cooled water droplets would impact onto the surfaces of the test models within the same duration of the icing experiment, resulting in less released latent heat of fusion associated with the phase changing (i.e., solidification) of the less super-cooled water mass collected by the test models. On the other hand, corresponding to the much colder ambient temperature under the rime icing condition (i.e., $T_\infty = -15\,°C$), the convective heat transfer process

(a). Over the test model with thermoplastic substrate   (b). Over the test model ith Aluminum substrate
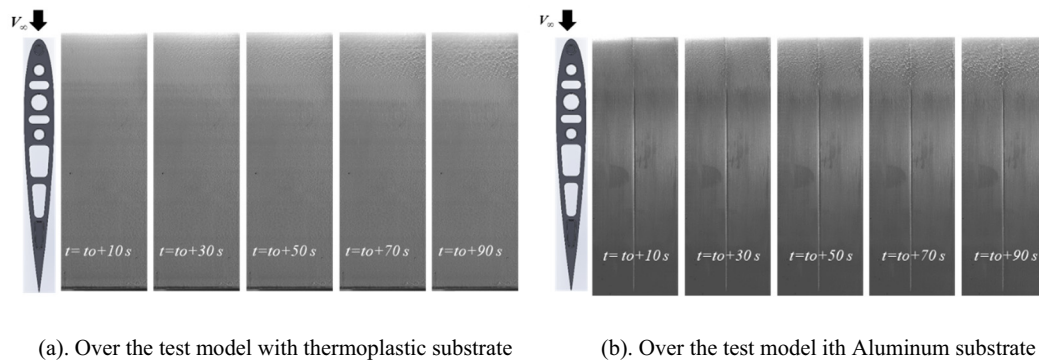
Fig. 7. Typical snapshot images to reveal the dynamic ice accretion process over the surfaces of the test airfoil/wing models under a typical rime icing condition of $V_\infty = 40$ m/s, $T_\infty = -15\,°C$, $LWC = 1.0$ g/m³.

(a). The test model with thermoplastic substrate   (b). The the model with Aluminum substrate
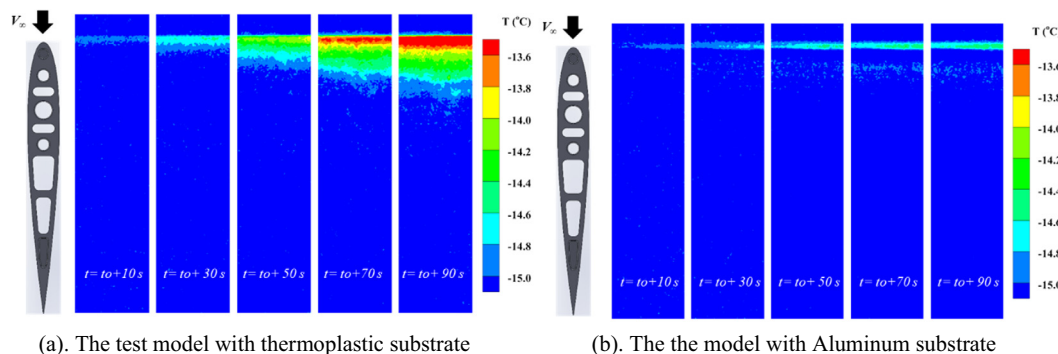
Fig. 8. Time evolution of the measured temperature distributions over the surfaces of the test airfoil/wing models under a typical rime icing condition of $V_\infty = 40$ m/s, $T_\infty = -15\,°C$, $LWC = 1.0$ g/m³.

via the boundary layer airflow over the surfaces of the test models was found to become much more significant, which could dissipate/remove the released latent heat of fusion very efficiently. As shown clearly in Figs. 7(a) and 8(a), even for the scenario with the minimized heat conduction to dissipate the released latent heat of fusion for the thermoplastic model, the convective heat transfer was still found to be able to dissipate/remove the released latent heat of fusion instantly. As a result, the super-cooled water droplets were found to be frozen into solid ice immediately upon impacting onto the test models.

By comparing the measured temperature distributions given in Fig. 8, the effects of the thermal conductivity of the airframe substrates (i.e., thermoplastic vs. Aluminum) on the dynamic ice accretion and unsteady heat transfer process over the surfaces of the two test models under the rime icing condition were revealed very clearly and quantitatively. As described above, while the dissipation of the released latent heat of fusion over the surfaces of the test models was found to be mainly accomplished by the convective heat transfer via the much colder airflow, the heat conduction via the airframe substrate was still found to play a noticeable role in dissipating/removing the released latent heat of fusion under the rime icing condition. As shown clearly in Fig. 8, even though the similar rime ice accretion processes were found to take place over the surfaces of the two compared test models, due to the much higher thermal conductivity of the Aluminum, a much faster dissipation of the released latent heat of fusion over the surface of the Aluminum model can still be observed. As a result, the surface temperature increases and the size of the "heated" region near the airfoil leading edge were found to be much smaller over the surface

of the Aluminum model, in comparison with those over the surface of the thermoplastic model.

Fig. 9 gives the measured profiles of the surface temperatures at the three representative locations over the surfaces of the two models as described above along with surface temperature distributions near the leading edge of the test models, which were extracted from the time sequences of acquired IR thermal images under the rime icing condition. It can be seen clearly that, corresponding to the continuous impingement of the super-cooled water droplets onto the surfaces of the test models to cause more and more latent heat of fusion being released associated with the phase changing of the impacted super-cooled water mass, the surface temperatures at the selected point "A" (i.e., at the airfoil leading edge) were found to increase monotonically with the ice accretion time for both the test model. Corresponding to the faster dissipation of the released latent heat of fusion due to the more intensive heat conduction via of the Aluminum airframe substrate, the increase rate of the surface temperature at the airfoil leading edge of the Aluminum model was found to be much smaller than that of the thermoplastic model. More specifically, as shown clearly in Fig. 9(b), while the surface temperature increase at the selected Point "A" on the surface of the thermoplastic model was found to reach to about 1.5 °C (i.e., $\Delta T_A \approx 1.5$ °C) after 80 s of the ice accretion (i.e., at $t = 80$ s), the corresponding value was found to be only about 0.5 °C (i.e., $\Delta T_A \approx 0.5$ °C) on the surface of the Aluminum model. Since no obvious surface water runback was observed over the surfaces of test models under the rime icing condition, the surface temperatures at further downstream locations (i.e., beyond the Point "B") were found to stay at almost the same

(a). Locations of the three selected points

(b). Measured temperature profiles at the three seleccted points

(c). Over the test model with thermoplastic substrate
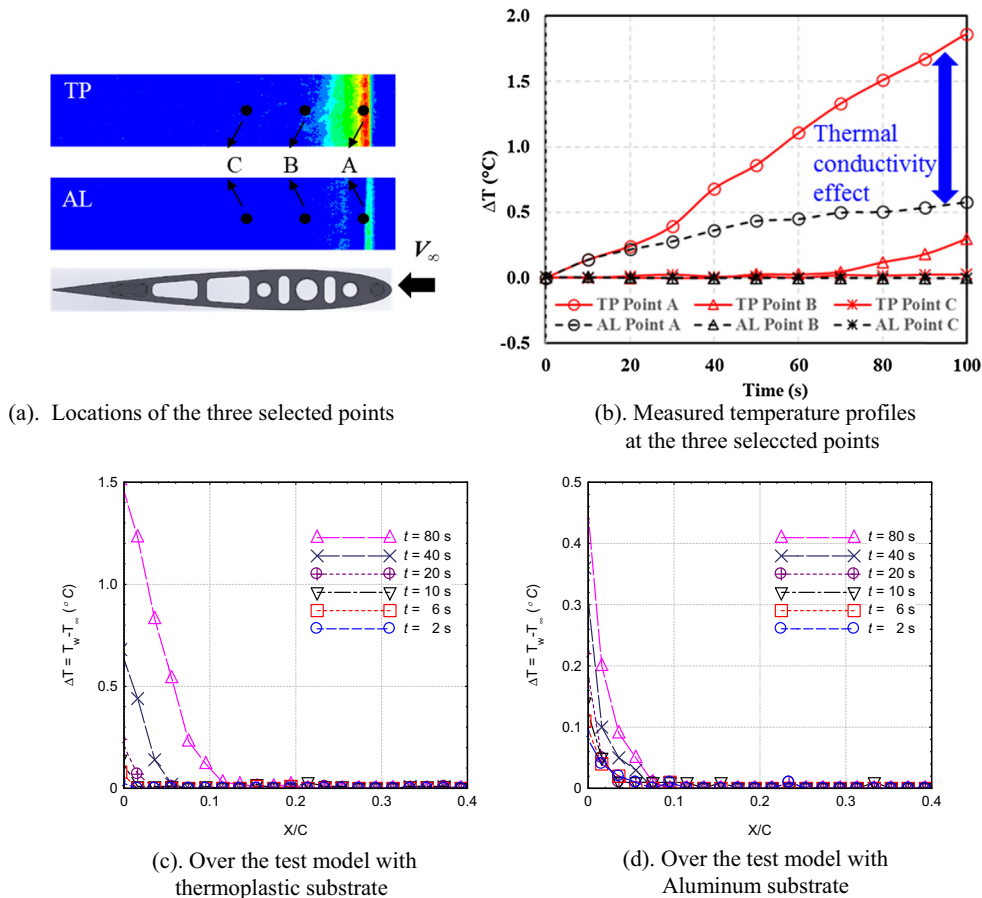
(d). Over the test model with Aluminum substrate

Fig. 9. Measured surface temperature profiles extracted from the IR thermal images for the test cases under a typical rime icing condition of $V_\infty = 40$ m/s, $T_\infty = -15$ °C and $LWC = 1.0$ g/m^3.

temperature as the incoming airflow (i.e., $\Delta T = T_W - T_\infty \approx 0$). It should also be noted that, the surface temperature at the selected point "B" (i.e., at the downstream location of 10% chord length) on surface of the thermoplastic model was found to increase slightly at the later stage of the icing experiment, i.e., at $t > 70$ s, as shown clearly in Fig. 9(b). The slight increase of the surface temperature at the selected point "B" on the thermoplastic model is believed to be caused by the slower dissipation of the released latent heat of fusion over the surface of the thermoplastic model as well as the enlarged direct impinging zone of the super-cooled water droplets associated with the substantial ice accretion over the surface of the thermoplastic model at the later stage of the icing experiment. In comparison, no such temperature increases at the further downstream locations were found over the surface of the Aluminum model within the entire time duration of the icing experiment.

5. Conclusion

In the present study, an experimental investigation was conducted to quantify the dynamic ice accretion and unsteady heat transfer process over the surface of a typical composite-based UAS wing model, in comparison to those over the surface of a conventional metal-based airfoil/wing model, in order to elucidate the underlying physics pertinent to UAS inflight icing phenomena. Two airfoil/wing models with the same chord length and the same NACA0012 airfoil profile, but being made of different materials (i.e., Aluminum vs. thermoplastic), were manufactured for the comparative study in order to evaluate the effects of the thermal conductivity of the airframe substrates on the dynamic ice accretion and unsteady heat transfer processes over the airframe surfaces. While the thermoplastic airfoil/wing model (i.e., the thermal conductivity of the thermoplastic material being ~0.2 W/m·K) is used to represent the composites-based UAS airframes, the Aluminum model with the thermal conductivity of the Aluminum substrate being ~200 W/m·K is used to represent the medal-based airframes of the conventional, large-sized, manned aircraft. The experimental study was performed in the Icing Research Tunnel of Iowa State University (i.e., ISU-IRT) with the two test models mounted side-by-side inside the ISU-IRT test section. During the experiments, in addition to recording the time evolution of the dynamic ice accretion process over the surfaces of the two compared test models with a high-speed imaging system, an infrared (IR) thermal imaging system was also utilized to measure the corresponding temperature distributions over the ice accreting airfoil surfaces. Based on the time sequences of the acquired snapshots of the ice accretion images and the spatially-and-temporally-resolved surface temperature measurements, the characteristics of the dynamic ice accretion and unsteady heat transfer processes over the surfaces of the two test models with different substrate materials, thereby, different thermal conductivity of the airframe substrate, were examined quantitatively under both typical wet glaze and dry rime icing conditions.

It was revealed clearly that, upon the impacting of the super-cooled water droplets carried by the frozen-cold airflow inside ISU-IRT, ice accretion was found to take place rapidly over the surfaces of the test models. A large amount of latent heat of fusion was found to be released associated with the phase changing (i.e., solidification) process of the impacted super-cooled water mass, causing the surface temperature increases and "heated" regions over the ice accreting surfaces of the test models. The dynamics of the ice accretion process (i.e., in the terms of the icing type and the resultant shape of the ice accretion) were found to be coupled closely with the unsteady heat transfer process to dissipate/remove the released latent heat of fusion over the ice accreting airfoil surfaces.

Under the typical wet glaze icing condition of $V_\infty = 40$ m/s, $T_\infty = -5$ °C, $LWC = 2.0$ g/m^3 for the present study, corresponding to the relatively high LWC level in the incoming airflow (i.e., $LWC = 2.0$ g/m^3), a tremendous amount of the latent heat of fusion was found to be released associated with the phase changing of the large amount of the super-cooled water mass collected on the surfaces of the test models. However, due to the relatively warm ambient temperature under such a glaze icing condition (i.e., $T_\infty = -5$°C), the heat transfer process could not be conducted fast enough to remove/dissipate all the released latent heat of fusion instantly, causing the local "accumulation" of the released latent heat of fusion over the ice accreting surfaces. As a result, only a portion of the impacted super-cooled water droplets were found to be frozen into solid ice immediately upon impacting onto the airfoil surfaces, while the rest of the impacted water mass was found to remain in the liquid phase, and run back quickly, as driven by the boundary layer airflow over the airfoil surfaces. The runback water was found to be frozen into solid ice eventually at much further downstream locations, i.e., beyond the direct impinging zone of the super-cooled water droplets, over the airfoil surfaces. Therefore, obvious surface water runback and the formation of rivulet-shaped ice structures were readily observed over the surfaces of the test models under the wet glazing condition. In comparison with that over the surface of the Aluminum model, the dissipation of the released latent heat of fusion on the surface of the thermoplastic model was found to be much slower, due to the much smaller thermal conductivity of the thermoplastic substrate. The slower dissipation rate of the released latent heat of fusion was found to result in much longer freezing time for the impacted super-cooled water mass to be frozen into solid ice, higher surface temperature increases over the airfoil surface; greater "heated" regions near the airfoil leading edge, and more obvious runback of the surface water reaching much further downstream locations (i.e., far beyond the direct impinging zone of the super-cooled water droplets), and formation of more complex, rivulet-shaped ice structures over the surfaces of the thermoplastic airfoil/wing model.

Under the typical rime icing condition of $V_\infty = 40$ m/s, $T_\infty = -15$ °C, $LWC = 1.0$ g/m^3 for the present study, much fewer super-cooled water droplets were found to be collected over the surfaces of the test models within the same duration of the icing experiment, resulting in less latent heat of fusion released over the airfoil/wing surfaces. On the other hand, the convective heat transfer process via the airflow over the surfaces of the test models was found to become much more effective to dissipate/remove the released latent heat of fusion, due to the much colder ambient temperature under the rime icing conditions (i.e., $T_\infty = -15$ °C). As a result, instead of forming transparent, smooth-looking glazy ice structures under typical glaze icing condition, much rougher and opaque ice layers were found to accrete mainly near the airfoil leading edges, i.e., within the direct impinging zone of the super-cooled water droplets, without any noticeable surface water runback over the airfoil surfaces. While the dissipation of the released latent heat of fusion over the surfaces of the test models was found to be accomplished mainly by the convective heat transfer under the rime icing condition, the heat conduction via the airframe substrate was still found to play a noticeable role in promoting the fast dissipation the released latent heat of fusion over the ice accreting airfoil surface. Even though the characteristics of the rime ice accretion process over the surfaces of the two compared test models were found to be very similar, the lower thermal conductivity of the thermoplastic airframe substrate was still found to cause a slower dissipation of the released latent heat of fusion, resulting in higher surface temperature and greater "heated" regions near the airfoil leading edge of the thermoplastic model, in comparison with those of the Aluminum model.

In summary, the thermal conductivity of an airframe substrate was found to affect the dynamic ice accretion and unsteady heat transfer processes over the surface of the airframe significantly. When operating under the same icing conditions, in comparison to those over the surfaces of the metal-based airframes used for conventional, large-sized manned aircraft, the lower thermal conductivity of the composite-based airframe substrates used by light-weight, Unmanned-Aerial-Systems (UAS) would cause a much slower dissipation of the released latent heat of fusion associated with the phase changing (i.e., solidification) of the impacted super-cooled water mass over the airframe surface, resulting in more obvious surface water runback and formation of more complex rivulet-shaped ice structures to cover much larger area over the surfaces of the UAS airframes. As a result, the aerodynamic performance degradation induced by the more complex ice accretion over the surfaces of the composite-based UAS airframes would be much more significantly. The findings derived from the present study highlight the importance and necessity to develop innovative and effective anti-/de-icing strategies tailored specifically for UAS icing mitigation and protection.

Conflict of interest

The authors declared that there is no conflict of interest.

Acknowledgments

Appendix A. Supplementary material

Supplementary data associated with this article can be found, in the online version, at https://doi.org/10.1016/j.ijheatmasstransfer. 2018.11.132.

References

[1] D. Weatherington, U. Deputy, Unmanned Aircraft Systems Roadmap, 2005–2030, 2005. <http://www.uadrones.net/military/research/acrobat/050713. pdf> (accessed October 16, 2016).

[2] P. Tran, G. Baruzzi, F. Tremblay, P. Benquet, FENSAP-ICE applications to unmanned aerial vehicles (UAV), in: 42nd AIAA Aerosp., Reno, Nevada, 2004, pp. AIAA-2004-0402. <http://arc.aiaa.org/doi/pdf/10.2514/6.2004-402> (accessed October 16, 2016).

[3] G. Botura, A. Fahrner, Icing detection system–conception, development, testing and applicability to UAVs, Goodrich Corp. AIAA, 2003. <http://arc.aiaa.org/doi/pdf/10.2514/6.2003-6637> (accessed October 16, 2016).

[4] K. Szilder, S. McIlwain, In-flight icing of UAVs – the influence of flight speed coupled with chord size, Can. Aeronaut. Sp. J. 58 (2012) 83–94, https://doi.org/10.5589/q12-007.

[5] B. Zhang, L. Tang, M. Roemer, Probabilistic weather forecasting analysis for unmanned aerial vehicle path planning, J. Guid. Control. Dyn. 37 (2014) 309–312, https://doi.org/10.2514/1.61651.

[6] R.B. Rutherford, De-ice and anti-ice system and method for aircraft surfaces, U.S. Patent No. 6,194,685, 2001.

[7] M. Pourbagian, W.G. Habashi, Aero-thermal optimization of in-flight electro-thermal ice protection systems in transient de-icing mode, Int. J. Heat Fluid Flow. 54 (2015) 167–182, https://doi.org/10.1016/j.ijheatfluidflow.2015.05.012.

[8] M. Vargas, J. Tsao, Observations on the growth of roughness elements into icing feathers, in: 45th AIAA Aerosp. Sci. Meet. Exhib., 2007, AIAA 2007-0900. <http://arc.aiaa.org/doi/pdf/10.2514/6.2007-900> (accessed October 8, 2015).

[9] C. Hochart, G. Fortin, J. Perron, A. Ilinca, Wind turbine performance under icing conditions, Wind Energy 11 (2008) 319–333, https://doi.org/10.1002/we.258.

[10] M. Bragg, G. Gregorek, J. Lee, Airfoil aerodynamics in icing conditions, J. Aircr. 23 (1986) 76–81. <http://arc.aiaa.org/doi/pdf/10.2514/3.45269> (accessed November 15, 2014).

[11] M.B. Bragg, A.P. Broeren, L.A. Blumenthal, Iced-airfoil aerodynamics, Prog. Aerosp. Sci. 41 (2005) 323–362, https://doi.org/10.1016/j.paerosci.2005.07.001.

[12] R.C. Henry, D. Guffond, Fran-atilde, O. Garnier, André, Bouveret, Heat transfer coefficient measurement on iced airfoil in small icing wind tunnel, J. Thermophys. Heat Transf. 14 (2000) 348–354.

[13] R.M. Waldman, H. Hu, High-Speed Imaging to Quantify Transient Ice Accretion Process over an Airfoil, J. Aircr. 53 (2016) 369–377, https://doi.org/10.2514/1.C033367.

[14] Y. Liu, H. Hu, An experimental investigation on the unsteady heat transfer process over an ice accreting airfoil surface, Int. J. Heat Mass Transf. 122 (2018) 707–718, https://doi.org/10.1016/j.ijheatmasstransfer.2018.02.023.

[15] F.P. Incropera, D. Dewitt, Fundamentals to Heat Transfer, John Wiley & Sons, 2002.

[16] C. Antonini, M. Innocenti, T. Horn, Understanding the effect of superhydrophobic coatings on energy reduction in anti-icing systems, Cold Reg. Sci. (2011). <http://www.sciencedirect.com/science/article/pii/S0165232X11000401> (accessed February 14, 2016).

[17] Y. Liu, L. Li, H. Li, H. Hu, An experimental study of surface wettability effects on dynamic ice accretion process over an UAS propeller model, Aerosp. Sci. Technol. 73 (2018) 164–172, https://doi.org/10.1016/j.ast.2017.12.003.

[18] R.M. Waldman, H. Li, H. Hu, An experimental investigation on the effects of surface wettability on water runback and ice accretion over an airfoil surface, in: 8th AIAA Atmos. Sp. Environ. Conf., 2016, https://doi.org/10.2514/6.2016-3139.

[19] J.T. Korhonen, T. Huhtamäki, O. Ikkala, R.H.A. Ras, Reliable measurement of the receding contact angle, Langmuir 29 (2013) 3858–3863, https://doi.org/10.1021/la400009m.

[20] Y. Liu, L.J. Bond, H. Hu, Ultrasonic-attenuation-based technique for ice characterization pertinent to aircraft icing phenomena, AIAA J. (2017) 1–8, https://doi.org/10.2514/1.J055500.

[21] M. Papadakis, R. Elangonan, G.A. Freund, M. Breer, G.W. Zumwalt, L. Whitmer, An Experimental Method for Measuring Water Droplet Impingement Efficiency on Two- and Three-Dimensional Bodies, 1989.

[22] D.M. Hawkins, T.A. Shannon, S.T. McClain, Convection from surfaces with real laser-scanned Ice accretion roughness and different thermal conductivities, 9th AIAA Atmos. Sp. Environ. Conf., American Institute of Aeronautics and Astronautics, Reston, Virginia, 2017, https://doi.org/10.2514/6.2017-3579.